

Article

Microstructure Evolution and Microstructural Characteristics of Al–Mg–Si Aluminum Alloys Fabricated by a Modified Strain-Induced Melting Activation Process

Chia-Wei Lin, Fei-Yi Hung *  and Truan-Sheng Lui

Department of Materials Science and Engineering, National Cheng Kung University, Tainan 701, Taiwan; QQkm0526@gmail.com (C.-W.L.); luits@mail.ncku.edu.tw (T.-S.L.)

* Correspondence: fyhung@mail.ncku.edu.tw; Tel.: +886-6-2757575-31395; Fax: +886-6-2346290

Received: 14 November 2017; Accepted: 19 December 2017; Published: 22 December 2017

Abstract: A modified strain-induced melting activation (SIMA) process is shown to improve high-temperature formability. The microstructural characteristics of the spheroidized grains of SIMA-processed alloys affect high-temperature formability. The effects of hot extrusion parameters and chemical composition on the evolution of spheroidized grains were investigated using several 6xxx series aluminum alloys subjected to a modified SIMA process. The results show that 6066 aluminum alloy is the most suitable alloy for the SIMA process, as it contains sufficient Mg, Si, Cu, and Mn. Adequate amounts of Mg, Si, and Cu lead to a high liquid fraction, and a sufficient addition of Mn inhibits grain growth. Proper hot extrusion parameters are essential, because initial fine and uniform recrystallized grains lead to fine and uniform globules. The phases at the global grain boundaries of 6066 aluminum alloy are eutectic phases of Al and Si, Al and Mg₂Si, and Al and Al₂Cu, as analyzed using transmission electron microscopy.

Keywords: Al–Mg–Si alloy; strain-induced melting activation (SIMA) process; spheroidized grains

1. Introduction

The semi-solid metal forming process is a hybrid net-shape process that combines the advantages of forging and casting [1,2]. Magneto-hydrodynamic casting, spray casting, and strain-induced melting activation (SIMA) are commonly used semi-solid processes for producing fine and globular grains that can enhance high-temperature formability [3,4]. The SIMA process is low-cost and utilizes stable procedures and simple equipment compared with other semi-solid processes such as magneto-hydrodynamic casting and spray casting [5,6]. The steps of common and traditional SIMA process are: (1) casting, which produces a dendritic structure; (2) hot work, which disintegrates the initial structure; (3) cold work, which introduces strain energy into the alloy; and (4) heat treatment, which makes the material recrystallize and partially melt at the temperature of solid–liquid coexistence. It is a three-step process because three steps of casting materials are required in order to obtain globular grains. A modified SIMA process, which has only two steps after casting, is used in the present study. Its flow is shown in Figure 1a. The two major differences between the traditional SIMA process and this modified SIMA process are: (1) this modified SIMA process uses severe hot extrusion instead of cold work to introduce a large amount of strain energy; and (2) this modified SIMA process uses a salt bath instead of an air furnace to improve heating uniformity and reduce heating time. Our previous research showed that this SIMA process can promote high-temperature compressibility and formability, and that the mechanical properties of SIMA-processed alloys are sufficiently high for practical applications after artificial aging [7–9]. Casting, hot extrusion, and salt bath (to attain

a regime in which solid and liquid phases coexist in equilibrium) [5,6] are the three major steps of this process. The microstructural evolution of this SIMA process is shown in Figure 1b. The initial state is a typical dendritic casting structure. The black dots in Figure 1b represent the secondary phase, whose melting point is low. After the alloys are subjected to hot extrusion, the microstructure changes to fine dynamic recrystallized grains. Then, the low melting point phases and parts of the eutectic composition start to partially melt and penetrate the grain boundaries of the recrystallized grains due to their high free energy in the salt bath step. This results in partially melted liquid phases surrounding the fine recrystallized grains. Finally, grain growth occurs and generates spheroidized grains in the salt bath because the surface energy of the global grains is low, and the restriction between solid grains disappears [2,3].

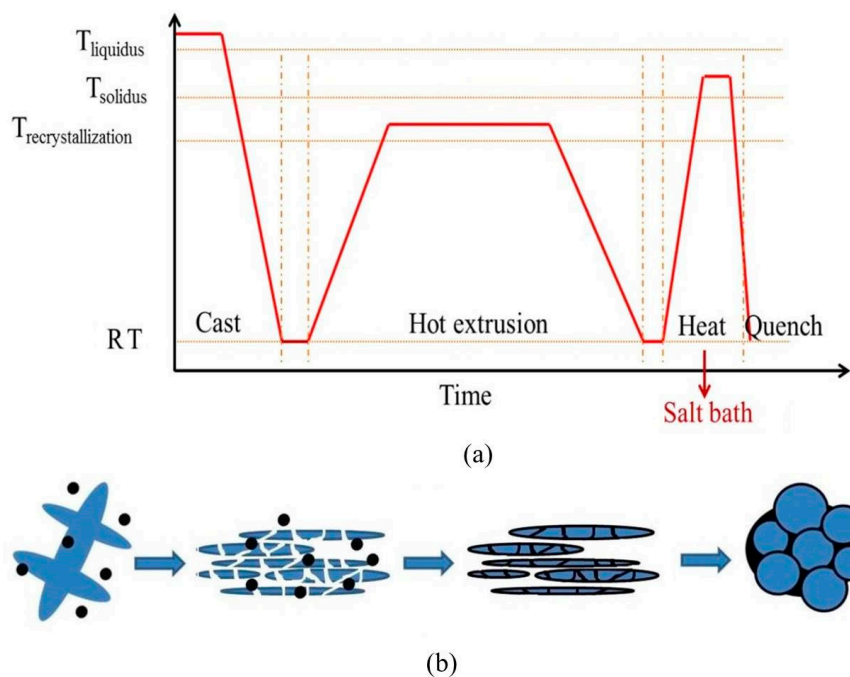


Figure 1. (a) Process flow and (b) mechanism of grain spheroidization of modified strain-induced melting activation (SIMA) process (RT: room temperature).

The major components of the 6xxx series aluminum alloys that are used in this study are Mg and Si. The Mg_2Si phase is generated first, since its forming free energy is lower than those of other precipitating phases [10–12]. The 6xxx aluminum alloys that have more Si than is required to form stoichiometric Mg_2Si commonly have relatively high strength and low ductility due to the hard and brittle Si particles in their matrix. In contrast, 6xxx aluminum alloys with excess Mg have relatively low strength and high ductility. Besides Mg and Si, Cu, Mn, Cr, Zr, Sc, and V are added to these alloys. Adding Mn inhibits grain growth, enhances strength, and increases recrystallization temperature [10,13,14]. Adding Cu improves strength and hardness due to the refining of the precipitated phase during artificial aging [15,16]. Adding Cr promotes corrosion resistance [13]. Adding Zr enhances strength, since Al_3Zr is generated and grain growth is inhibited, and adding Sc or V retards grain growth [17,18].

In this research, several extruded 6xxx aluminum alloys were used to investigate the effects of components and hot extrusion parameters on spheroidized grains in the modified SIMA process. The purpose is to understand how to design an alloy that is suitable for this SIMA process. Moreover, the nanoscale microstructural characteristics, phases at globular grain boundaries, and mechanism of elemental diffusion are analyzed using transmission electron microscopy (TEM).

2. Materials and Methods

Table 1 shows the codes and compositions of the seven materials used in this research. The compositions are analyzed by glow discharge spectrometer (GDS) (GDS-750 QDP, LECO Corporation, St. Joseph, MI, USA). The salt bath temperature was 620 °C based on previous research studies [7–9]. All of the materials were extruded sheets except for 6069-rod, which was an extruded rod. Notably, all of the materials were extruded from a six-inch diameter casting rod, in other words, the extruded sheets with same thickness have an identical extrusion ratio (the same amount of deformation). 6061 and 6061-Mn were used for discussing the effect of Mn addition; their thickness is 3 mm and their extrusion ratios were identical. The 6066-3mm and 6066-9mm sheets were used for determining the effect of strain introduced by hot extrusion, because their original castings alloy are the same. A 6069-sheet with 3 mm thickness and a 6069-rod with 28 mm diameter were used for understanding the effect of extrusion shape. The effect of strain also can be analyzed due to the amount of strain at the edge of the rod being larger than that in center of rod. Finally, 6061, 6066, 6069, and 6082 (with 3 mm thickness, too) aluminum alloys were used for determining the effect of composition by observing their microstructural evolution. Optical microscopy (OM) (BX41M-LED, Olympus, Tokyo, Japan), scanning electron microscopy (SEM) (JSM-7000 & JSM 7001, JEOL, Peabody, MA, USA), and an electron probe X-ray microanalyzer (EPMA) (JEOL, Peabody, MA, USA) were used for investigating and analyzing the microstructural evolution, microstructural characteristics, and elemental distribution. The goal was to determine principles for designing alloys suitable for the SIMA process.

Table 1. Compositions of Al–Mg–Si alloys used in this research (Unit: wt %).

Code	Mg	Si	Cu	Mn	Fe	Cr	V	Zr	Al
6061	0.88	0.67	0.16	0.03	0.19	0.04	0	0	Bal.
6061-Mn	0.83	0.75	0.20	0.31	0.19	0.07	0	0	Bal.
6066-3mm	1.02	1.29	0.95	1.02	0.19	0.18	0	0	Bal.
6066-9mm	1.02	1.29	0.95	1.02	0.19	0.18	0	0	Bal.
6069-sheet	1.25	0.75	0.73	0.05	0.13	0.16	0	0.11	Bal.
6069-rod	1.30	0.85	0.72	0.09	0.13	0.14	0.12	0	Bal.
6082	0.71	1.10	0.06	0.71	0.19	0.23	0	0	Bal.

After the most suitable alloy was determined, more detailed microstructural analyses were conducted using TEM. The TEM samples were prepared using a focused ion beam (FIB).

3. Results and Discussion

3.1. Effects of Extrusion Conditions and Chemical Composition on Microstructure

The concept of an equivalent circle is used in this study. When the shape of a grain is not circular in a two-dimensional plane, grain size is represented by the diameter of the equivalent circle, as shown in Figure 2. The size and appearance of globular grains are affected by the initial extrusion state and alloy composition. The microstructures of the initial extruded alloys used in this research are shown in Figure 3. Their initial grain sizes are shown in Table 2.

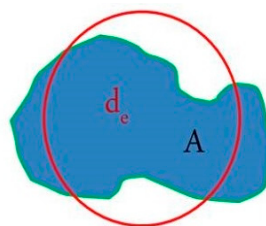


Figure 2. Definition of equivalent circle diameter.

Even though the extrusion ratios of 6061 and 6061-Mn are identical, the initial grain size of 6061 is larger than that of 6061-Mn. Dynamic recrystallization occurred in both aluminum alloys in the hot extrusion step, but the grain sizes of the two alloys are not identical due to Mn retarding grain growth after dynamic recrystallization, since it increases the temperature of recrystallization [10,13,14].

As the extrusion ratio was increased, the level of dynamic recrystallization increased. This can be shown by comparing the microstructures of 6066-3mm and 6066-9mm. The higher level of recrystallization of 6066-3mm led to a more uniform and smaller initial grain size. Besides, dynamic recrystallization in 6061 alloys should be easier than that in 6066-3mm alloys due to the addition of Mn, which increases recrystallization temperature [10,13,14].

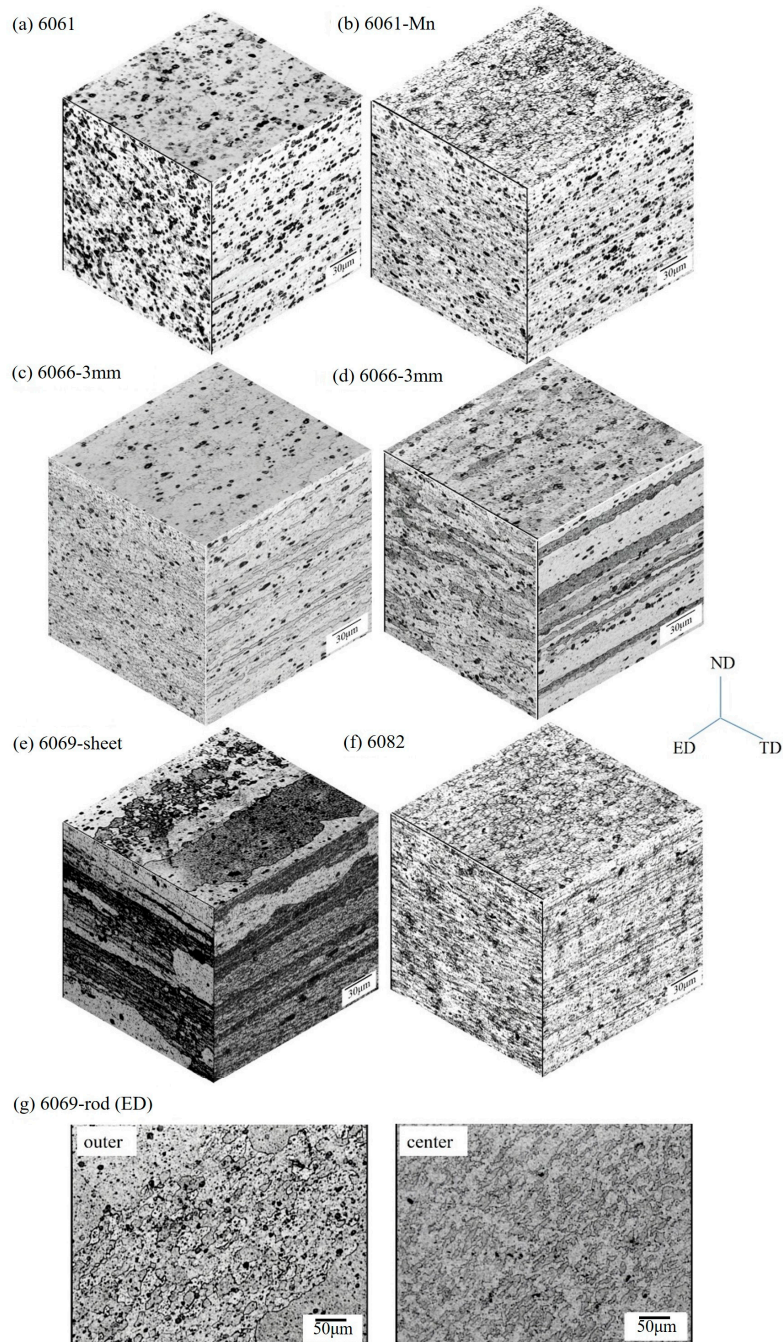


Figure 3. Microstructures of extruded Al-Mg-Si alloys. (a) 6061; (b) 6061-Mn; (c) 6066-3mm; (d) 6066-9mm; (e) 6069-sheet; (f) 6082 and; (g) 6069-rod.

Table 2. The average initial grain size, liquid fraction, and growth rate of Al–Si–Mg alloys.

Code	Average Initial Grain Size (μm)	Liquid Fraction (%) in 10-min Salt Bath	K ($\mu\text{m}^3 \cdot \text{min}^{-1}$)
6061	40	3.2	42,329
6061-Mn	7	7.2	30,054
6066-3mm	3–5	16	16,806
6066-9mm	5–7	15.5	17,024
6069-sheet	7 & 300	10.4	31,579
6069-rod (center)	15	11.2	32,678
6082	8	7.5	24,357

Both coarse and fine grains can be seen in 3-mm thick 6069-sheet alloys. The coarse grains located near the surface resulted from the high friction heat at the alloy surface. The coarse grains located in the center zone of the sheets resulted from similar crystal orientations of neighboring grains. According to the grain coalescence mechanism, if the crystal orientations of neighboring grains are similar, the grains will easily merge, forming coarse grains. This led to the non-uniform grain distribution in 6069-sheet. In the 28-mm diameter 6069-rod alloy, fine grains appear in the center, and coarse and fine grains appear at the edge. This is due to the lower strain in the center of the rod creating a smaller driving force for grain growth, and the higher strain at the edge of the rod making some crystals with similar orientations grow and then merge. The initial grains of 6069 alloys are easier to grow than other alloys, except for 6061 alloy, because Mn is not added. Besides, although the 6069-sheet and 6069-rod did not contain Mn, the level of grain growth of the 6069 alloys was lower than that of the 6061 alloys due to the addition of V and Zr.

Equiaxial grains resulted from the dynamic recrystallization in the 3-mm thick 6082 alloy, which was due to the Mn content. This confirms that Mn inhibits grain growth.

3.2. Microstructural Evolution of SIMA-Processed Alloys

The microstructural evolution in the salt bath step for all of the alloys is shown in Figure 4. The codes of specimens subjected to a salt bath are marked with the prefix “SB”. The salt bath time was set as 1 min, 10 min, or 30 min. After the salt bath, grains were spheroidized, and grain boundaries were broadened due to the low melting point phases melting and penetrating the grain boundaries. With grain growth, the melting phases aggregated to form liquid pools [3,4]. The alloys fabricated by the modified SIMA process presented in this research are defined as SIMA alloys. The area ratio of these melting phases that solidified after cooling is defined as the liquid fraction. With forming at high temperature, these phases melt again, improving formability [7–9]. Table 2 shows the liquid fraction of all of the other alloys after a salt bath at 620 °C for 10 min. All of the data were calculated using ImageJ software and averaged from at least three images. Fine grains, a high degree of spheroidization, and a high liquid fraction are the major factors for promoting high-temperature formability [7–9].

In general, globular grain growth is based on Lifshitz–Slyozov–Wagner (LSW) theory [3,4,19,20]. The formula is $d^n - d_0^n = Kt$, where d is the average grain size, which depends on salt bath duration, d_0 is the initial grain size, t is the salt bath duration, K (units: $\mu\text{m}^3 \cdot \text{min}^{-1}$) is the coarsening rate constant, and exponent n is determined by the diffusive mechanism of grain growth. For $n = 3$, the mechanism of grain growth is Ostwald ripening. The theoretical formula can be rewritten as $d^3 = Kt + d_0^3$. Ostwald ripening is the major mechanism of globular grain growth of SIMA alloys when the liquid fraction is sufficient [21]. Ostwald ripening is a diffusion-controlled mechanism. Large grains become larger, and small grains become smaller (even disappearing). In this paper, it is assumed that the grain growth mechanism of all of the materials is Ostwald ripening for comparing the grain growth rate.

The calculated grain growth rates are shown in Table 2. The grain growth rate of 6061-Mn is lower than that of 6061, and those of the 6066 and 6082 alloys are lower than those of the other alloys. This might result from different liquid fraction and adding Mn, since it decreases the rate of globular grain growth.

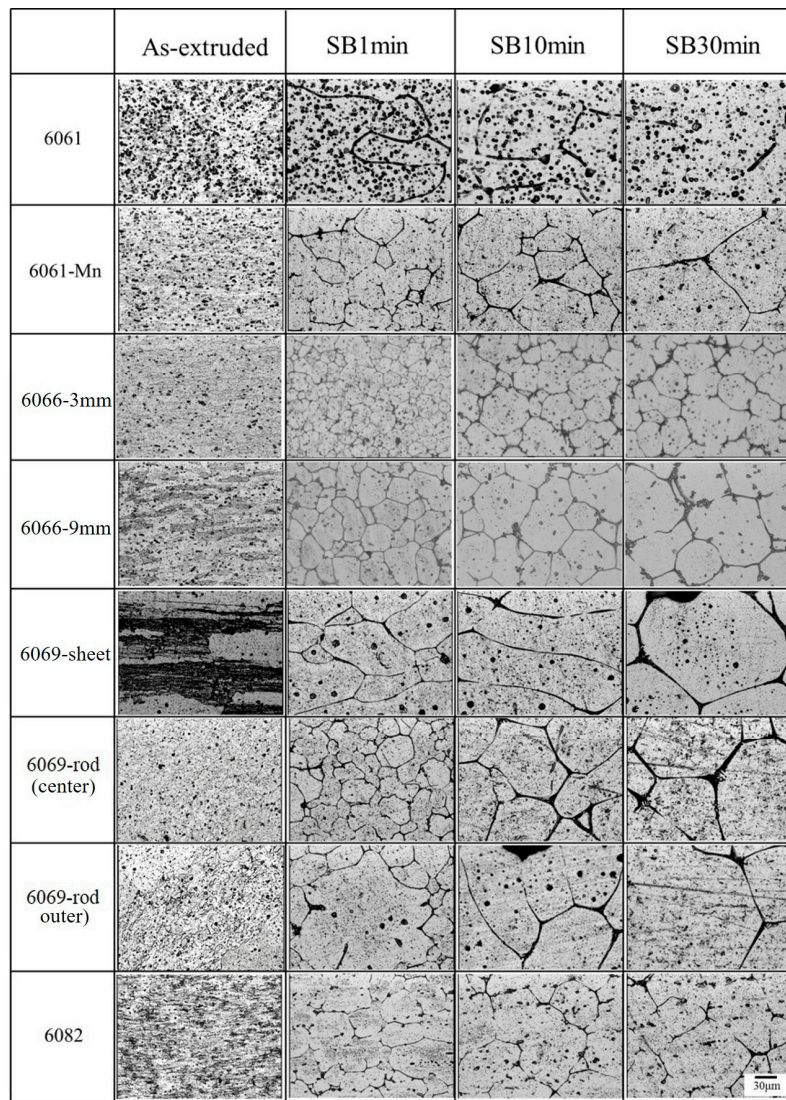


Figure 4. Microstructural evolution of Al-Mg-Si alloys via salt bath.

After the salt bath, the grain size of 6066-3mm is smaller than that of 6066-9mm, even though their grain growth rates K are almost identical, as shown in Table 2. This indicates that the initial grain size at the extrusion state affects the spheroidized grain size of SIMA alloys. In other words, finer and more uniform dynamic recrystallized grains are beneficial for obtaining smaller and more uniform spheroidized grains. The same result was found in the center of the 6069-rod. Its small and uniform initial recrystallized grains led to fine and uniform spheroidized grains.

Table 2 also shows the liquid fractions of the four kinds of aluminum alloy during the 10-min salt bath. The liquid fractions are those for, in order, 6066, 6069, 6082, and 6061 (from high to low). The liquid fractions of a given alloy are similar, except for 6061. In general, the liquid fractions of a given alloy should be similar. However, the high grain growth and low liquid fraction of the 6061 alloys led to their respective positions affecting the results.

The degrees of spheroidization of all of the alloys are shown Figure 4. The degrees of spheroidization of the 6066 alloys and 6069-rod are higher than those of the other samples. The grains of the 6061 and 6069-sheet are non-equiaxed, because the initial coarse grains, and the globular grain boundaries of the 6082 alloys cannot be connected due to the low liquid fraction. Therefore, their degrees of spheroidization are relatively low. The degrees of spheroidization of the 6066-3mm sheet, 6066-9mm

sheet, and 6069-rod are highest due to their fine and uniform initial recrystallized grains and high liquid fraction.

The elemental distributions obtained using EPMA are shown in Figure 5. Mg, Si, and Cu are the major elements located at grain boundaries, and Fe, Mn, Cr, and V exist in the particle phases. It indicates that the melting phases in the salt bath step are mostly composed of Mg, Si, Cu, and Al. The three phase diagrams in Figure 6 show that the eutectic points of Al and Si, Al and Mg₂Si, and Al and Al₂Cu are 577 °C, 595 °C, and 548 °C, respectively. Moreover, Table 3 shows the probable maximum weight percentages of Mg₂Si, Al₂Cu, excess Si, and the sum of these three phases for Al–Mg–Si alloys. They are calculated from the GDS analysis, as shown in Table 1. The order of the sums of these phases is those for 6066, 6069, 6082, and 6061 (from high to low). This order is consistent with the order for the liquid fractions shown in Table 2. These results show that the major phases distributed at globule boundaries are these three phases.

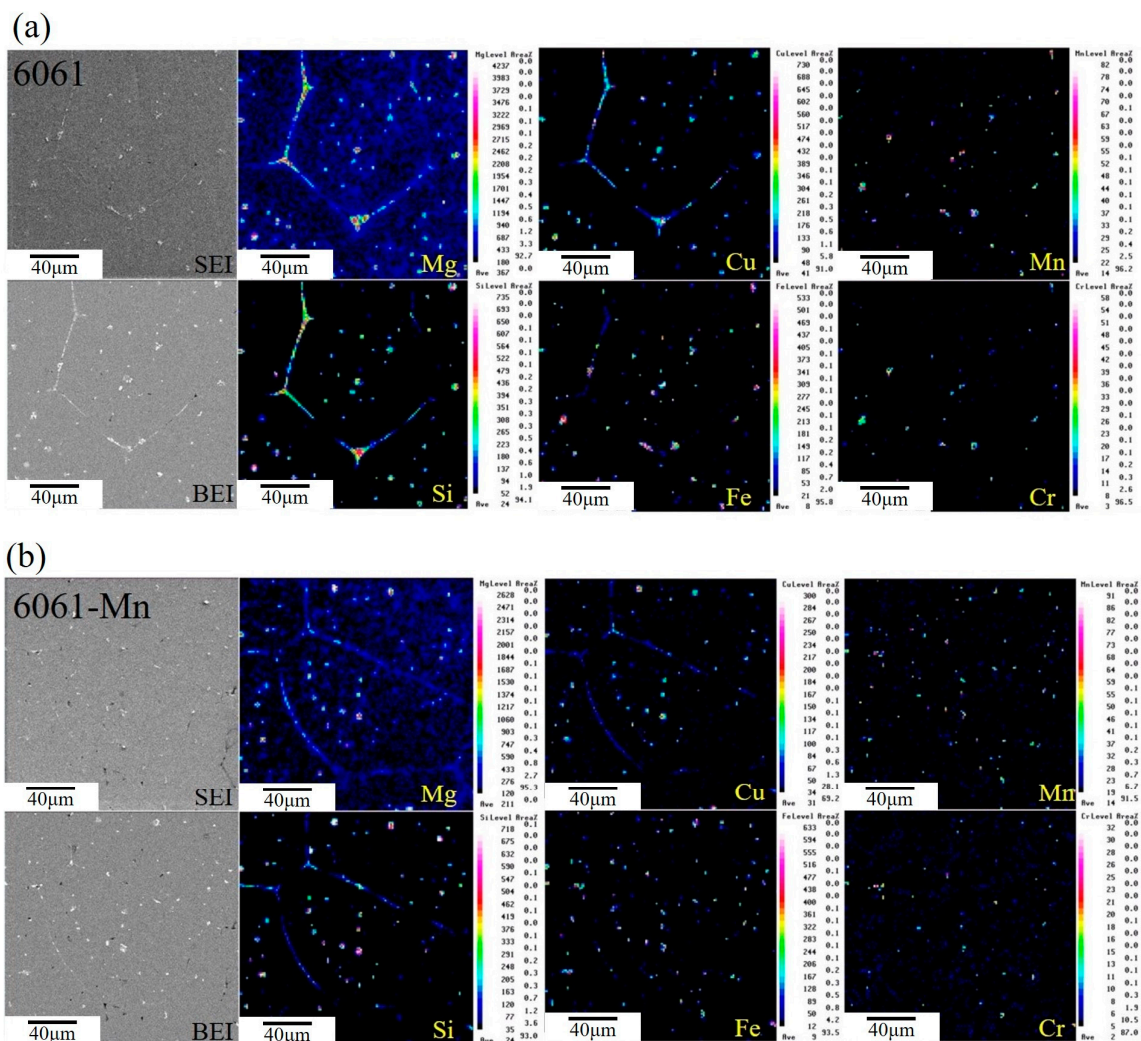


Figure 5. Cont.

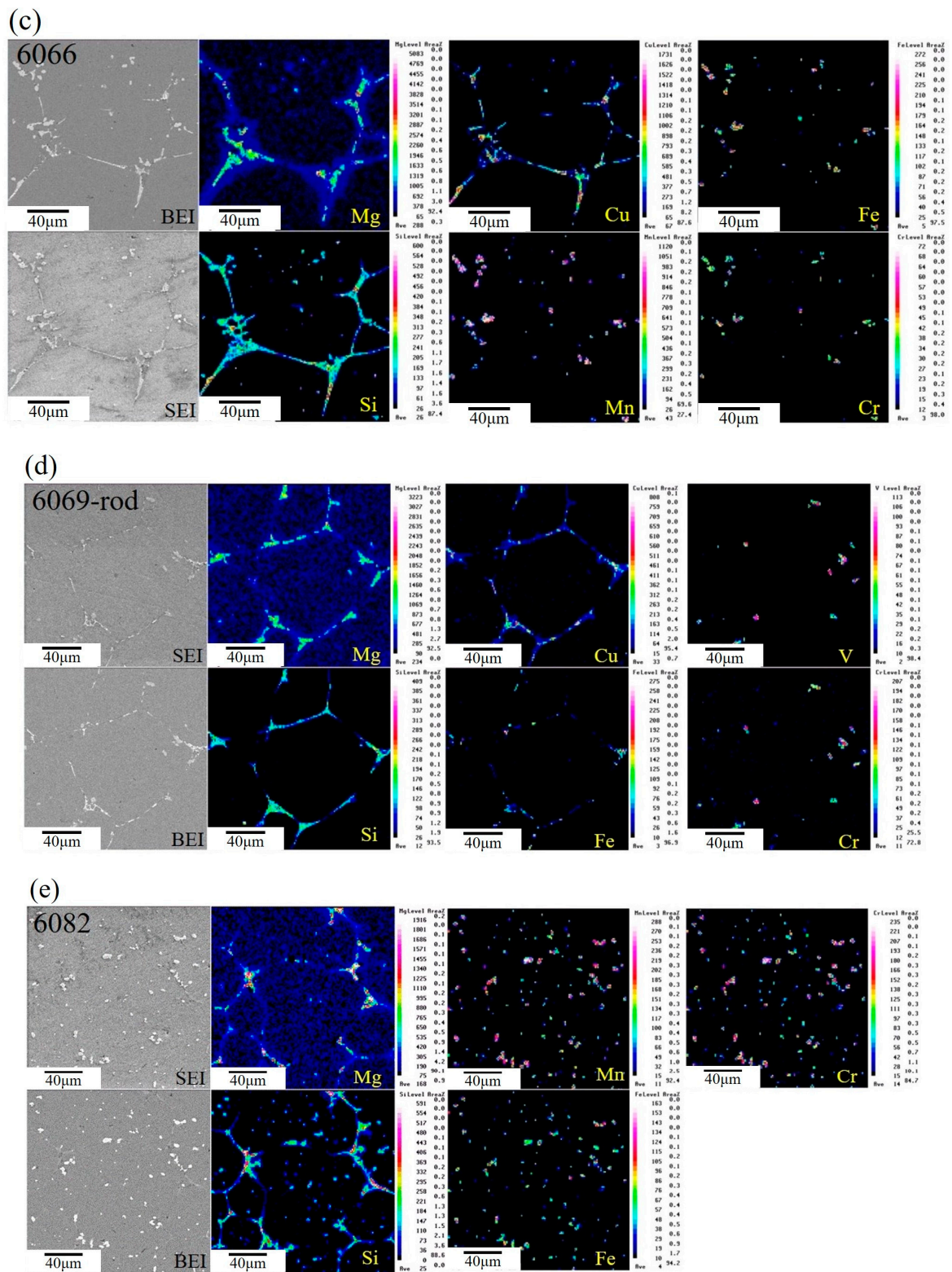


Figure 5. Elemental distribution in Al–Mg–Si alloys: (a) 6061; (b) 6061-Mn; (c) 6066; (d) 6069-rod and (e) 6082.

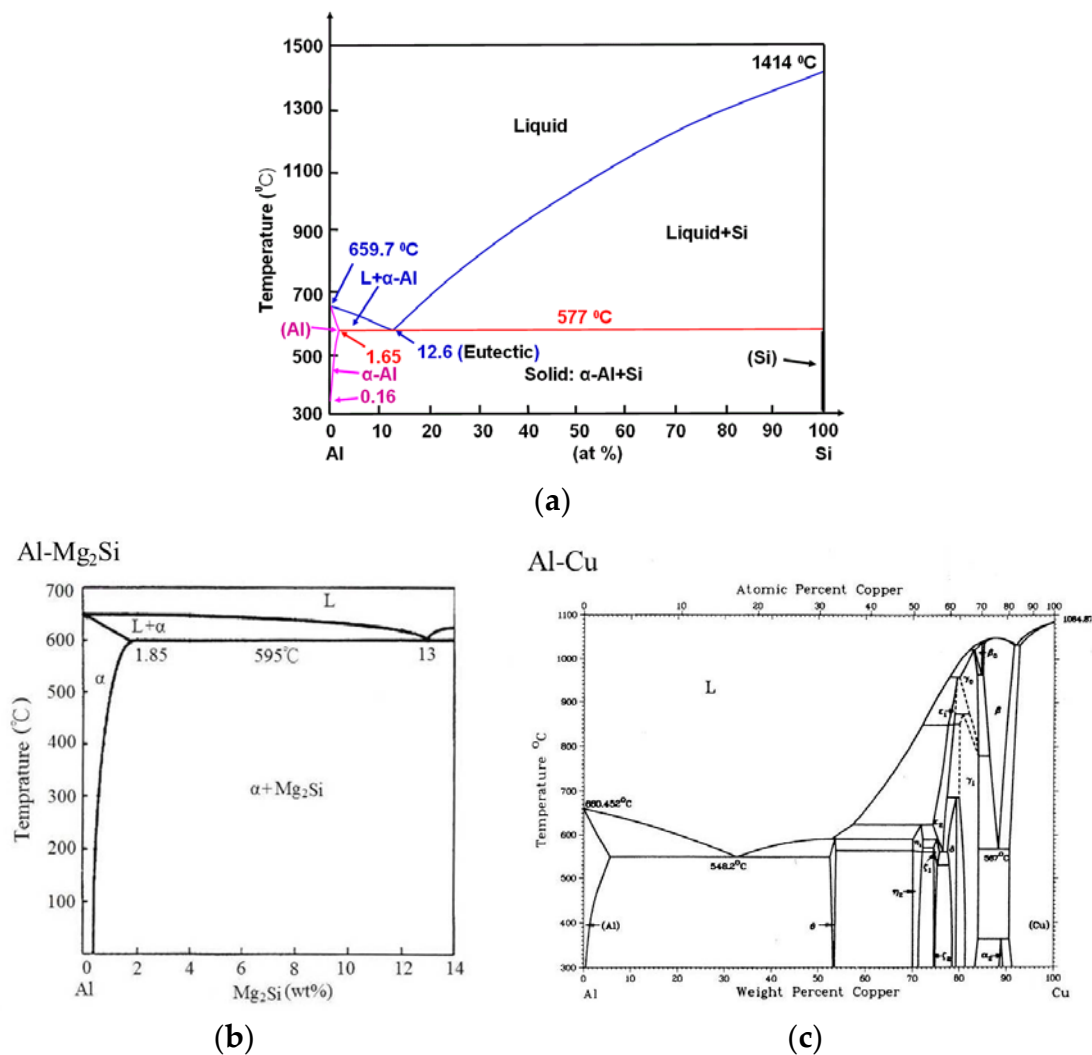


Figure 6. Phase diagrams of (a) Al-Si; (b) Al-Mg₂Si; and (c) Al-Cu.

Table 3. Weight ratios of Mg₂Si and Al₂Cu in Al-Mg-Si alloys (wt %).

Material	Mg ₂ Si	Al ₂ Cu	Excess Si	Sum
6061	1.11	0.33	0.28	1.72
6066	1.61	1.76	0.7	3.97
6069	2.01	1.35	0.07	3.43
6082	1.12	0.11	0.7	1.93

Three main factors affect the generation of fine, uniform, and highly spheroidized globular grains with high liquid fractions in this modified SIMA process: (1) a proper composition with sufficient elements (e.g., Mg, Si, and Cu) that can form low melting point phases is necessary in order to enhance the liquid fraction for 6xxx series aluminum alloys; (2) the initial extrusion microstructure should be fine and uniform grains for generating fine and uniform spheroidized grains after the salt bath; (3) particular elements (e.g., Mn, V, and Zr) should be added to inhibit grain growth, not only to create fine recrystallized grains in the hot extrusion step, but also to create fine spheroidized grains in the salt bath step.

In this study, 6066 aluminum alloy was found to be the most suitable material for obtaining finest and most spheroidized globules. Therefore, 6066 alloy was used in the subsequent microstructural analyses with TEM.

3.3. Microstructural Characteristics of Phases Located at Globule Boundaries in SIMA-Processed 6066 Alloy

The results of energy-dispersive X-ray spectroscopy (EDS) for phases located at globule boundaries are shown in Figure 7. The image is the backscattered electron image (BEI) of a SEM micrograph. Three phases can be seen. The brighter globule boundary phases marked by *b* are mainly composed of Si and Cu. The darker particles marked by *c* at the grain boundaries and in liquid pools are mostly composed of Si and Mg. Moreover, Si, Mn, Cr, and Fe are the major elements of the brighter equiaxed particles at the grain boundaries and in the grain interior (marked by *a*). In this study, FIB was adopted to cut the TEM samples. A liquid pool was obtained with Mg and Si-rich phases and Cu-rich boundaries, two areas that are major positions for nanoscale microstructural observation.

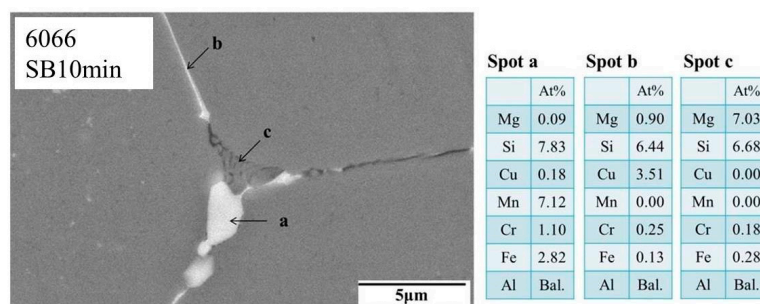


Figure 7. Energy-dispersive X-ray spectroscopy (EDS) analysis of phases at globule boundaries in SIMA-processed 6066 alloy.

3.3.1. TEM Analysis of Liquid Pool Mostly Composed of Si and Mg

The liquid pool is composed of eutectic phases and is a layer-by-layer structure in the BEI image. Figure 8 shows the liquid pool morphology observed by TEM. Two phases can be seen. One phase is similar to a river, which is distributed in the other phase. The results of composition analysis by EDS are shown in Figure 8B. Four phases can be observed. The river-like phase *a* is composed of Mg and Si, and is likely Mg_2Si . Phase *b* is likely the Al matrix. It can be speculated that phases *a* and *b* are the eutectic phase of Al and Mg_2Si . Phase *c*, the neighboring phase of *a*, is composed of Al and Cu, and is likely Al_2Cu . The composition of the large particle phase *d* is similar to that of phase *c* in Figure 7. It is composed of Si, Mn, Cr, Fe, and Al. According to the diffraction pattern shown in Figure 8C and EDS results, phase *d* is face-centered cubic $Al_{15}(Fe, Mn, Cr)_3Si_2$. Its melting point is close to 660 °C [22]. Therefore, this phase distributes uniformly in the alloys instead of melting and locating at globule boundaries. When the duration of the salt bath increases, its particle size increases. The coarsening mechanism of that phase follows the Gibbs–Thomson effect to reduce the total surface energy. Small particles aggregated together to form a large particle phase.

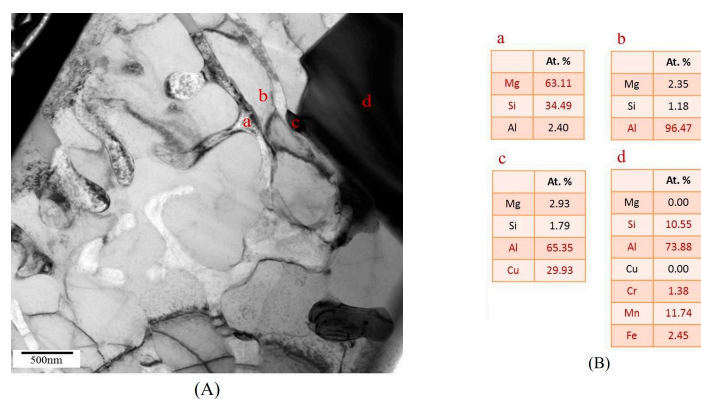


Figure 8. Cont.

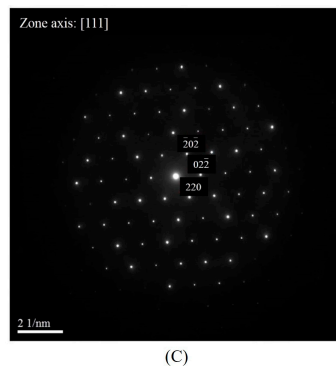


Figure 8. (A) Morphology of resolidified liquid phases; (B) composition of phases analyzed by EDS; and (C) diffraction pattern of phase *d*.

The selective area diffraction patterns of phases *a* and *b* in Figure 8 are shown in Figure 9. Phase *a* is face-centered cubic Mg_2Si , and phase *b* is face-centered cubic aluminum matrix. Notably, according to the overlapping figure, the (220) crystal orientation of Mg_2Si and the (200) crystal orientation of Al are the same. This indicates that the crystal orientations of these two phases are coherent.

Phase *c* in Figure 8 neighbors Mg_2Si . The same phenomenon can be seen in Figure 10. The EDS results show that phase *c* is composed of Al and Cu. The selective area nanobeam diffraction pattern indicates that this phase is tetragonal Al_2Cu . The solidification of Mg_2Si occurs before that of Al_2Cu due to the solidification temperature of Mg_2Si being higher than that of Al_2Cu . This led to the obvious interface between Mg_2Si and Al_2Cu .

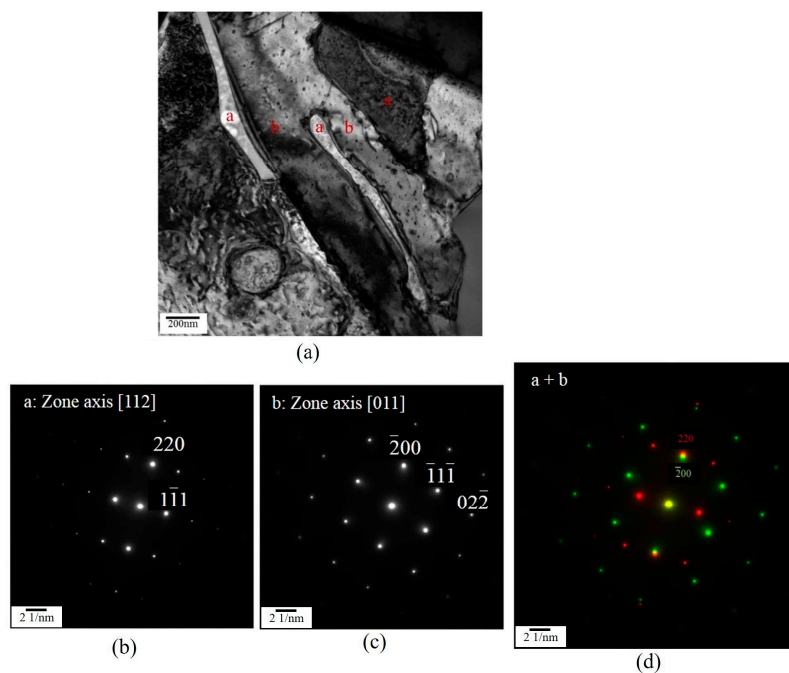


Figure 9. Coherence between Mg_2Si and the Al matrix. (a) morphology of Mg and Si-rich globule boundary; (b) diffraction patterns of phases *a*; (c) diffraction patterns of phases *b*; (d) merging diffraction patterns of phases *a* and *b*.

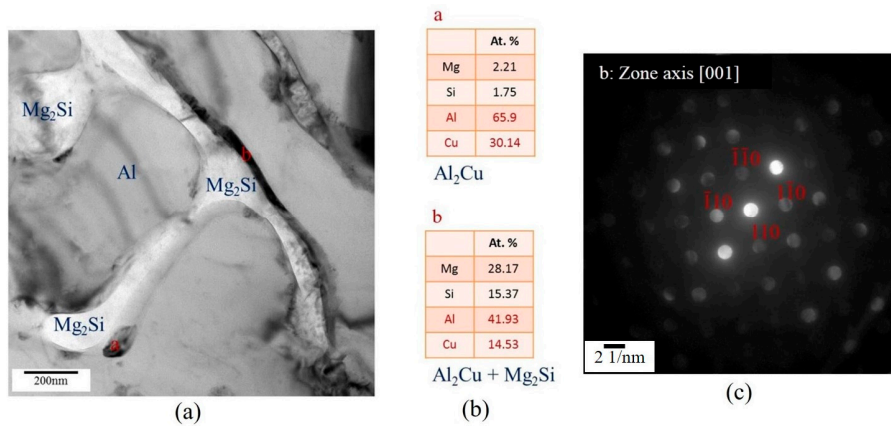


Figure 10. Analysis of Al₂Cu in liquid pool. (a) morphology of globule boundary; (b) composition of phases analyzed by EDS; (c) diffraction pattern of phase *b*.

3.3.2. TEM Analysis of Globule Boundaries Mostly Composed of Si and Cu

Figure 11 shows the microstructure investigated by TEM of Cu-rich globule boundaries. Al grains are surrounded by a ribbon-like phase, which is composed of globule boundaries. At high magnification, it can be seen that the ribbon-like phase is composed of a large number of fine piece-like phases and some particle phases. The piece-like phases are the tetragonal Al₂Cu phase, as determined from the selective area diffraction pattern. The boundaries are formed by Al₂Cu and Al eutectic solidification.

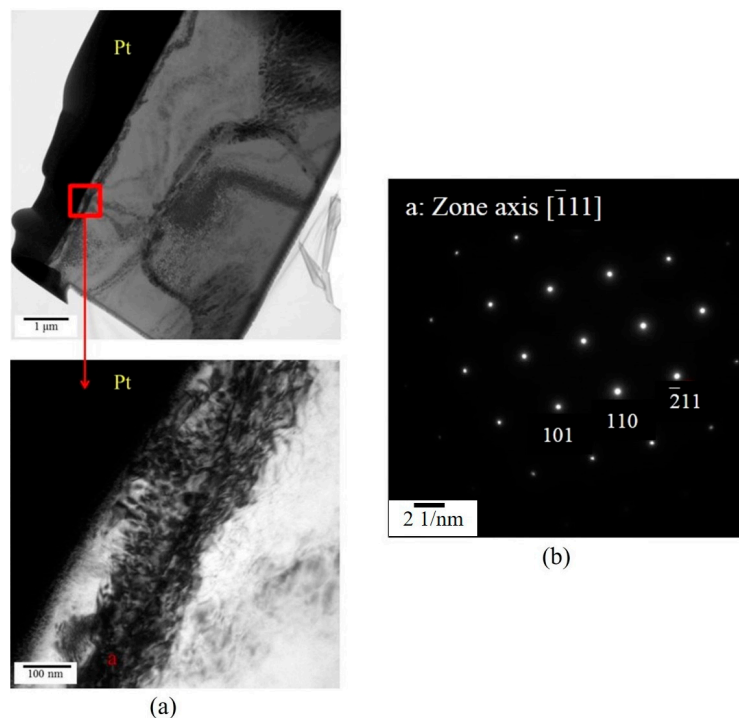


Figure 11. Analysis of Al₂Cu phase at Cu-rich globule boundaries. (a) morphology of Cu-rich globule boundary and (b) diffraction pattern of phase located at Cu-rich globule boundary.

Diffraction patterns taken at three points of the Al₂Cu phase are shown in Figure 12a. They are the same phase (Al₂Cu), and their orientations are rotated by a slight angle with respect to each other as shown in Figure 12b because of a high cooling rate (water quenching). Figure 12c confirms the phase

is Al_2Cu . The high cooling rate resulted in the immediate generation of a large number of crystals of Al_2Cu .

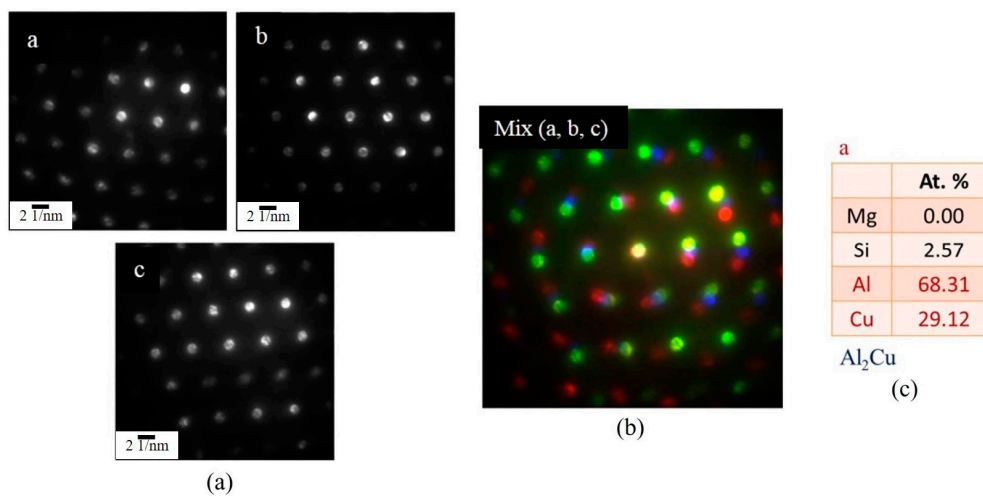


Figure 12. Diffraction patterns of phases at Cu-rich globule boundaries (a) diffraction patterns taken at three points (a, b and c); (b) merging of above three diffraction pattern; (c) composition of phases analyzed by EDS.

The EDS results in Figure 8 show that the Cu-rich globule boundaries are not only composed of Al and Cu, but also Si. A large number of Si particles exist at the boundaries, as shown in Figure 13. The arrows in Figure 13 indicate Si particles identified from EDS. In this figure, spot *a* is composed of Al grains and Si particles, spot *b* is composed of Al_2Cu and Si particles, and spot *c* is composed Al and Al_2Cu . These results prove that the eutectic phases of Al and Si, whose melting points are below the temperature of the salt bath, existed at the globule boundaries.

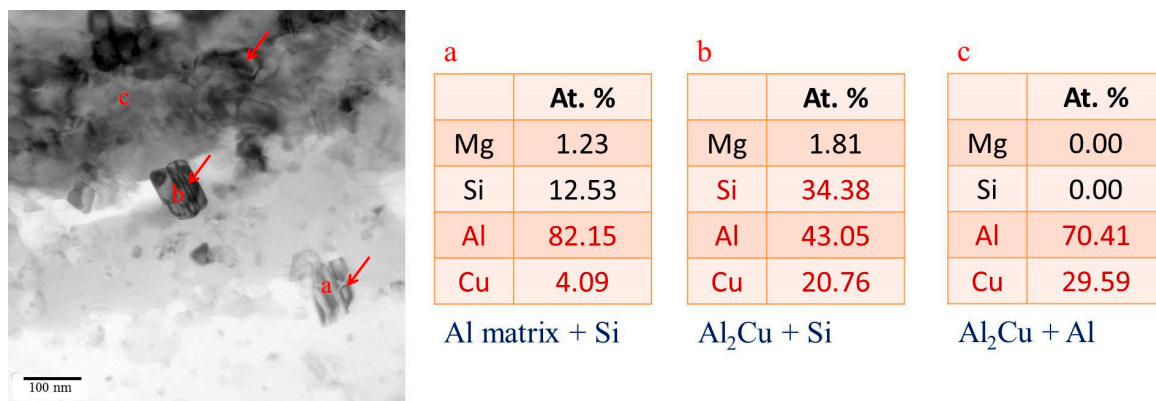


Figure 13. EDS analysis of eutectic Si particles.

TEM data exhibit phases on the globule boundaries of SIMA-processed 6066 aluminum alloy are the eutectic phases of Al and Mg_2Si , Al and Al_2Cu , and Al and Si. This is consistent with the EPMA data.

4. Conclusions

The following conclusions were drawn based on the results and discussion.

1. Three major factors affect the generation of fine, uniform, and highly spheroidized globular grains with high liquid fractions in this modified SIMA process: (a) sufficient elements to form

- low melting point phases; (b) the addition of particular elements for inhibiting grain growth; and (c) proper extrusion parameters to get a fine and uniform initial extrusion microstructure.
- Of the 6xxx series alloys, 6066 aluminum alloy is the most suitable for the modified SIMA process. Mg, Si, and Cu can generate low melting point phases, and Mn can inhibit grain growth.
 - According to TEM results, the eutectic phases of Al and Mg₂Si, Al and Al₂Cu, and Al and Si are the major phases at the globule boundaries. EPMA data confirm this result. The high melting-point phase Al₁₅(Fe,Mn,Cr)₃Si₂ was also identified by TEM.

Acknowledgments: The authors are grateful to the Instrument Center of National Cheng Kung University and the Ministry of Science and Technology of Taiwan (NSC MOST103-2221-E-006-056-MY2) for their financial support.

Author Contributions: C.-W.L. designed experiments majorly, performed the experiments, analyzed the data and wrote the paper, F.-Y.H. and T.-S.L. contributed materials/lab/analysis tools and gave suggestions for improving this research.

Conflicts of Interest: The authors declare no conflicts of interest.

References

- Fan, Z. Semisolid metal processing. *Int. Mater. Rev.* **2002**, *47*, 49–85. [[CrossRef](#)]
- Tzimas, E.; Zavaliangos, A. A comparative characterization of near-equiaxed microstructures as produced by spray casting, magnetohydrodynamic casting and the stress induced, melt activated process. *Mater. Sci. Eng. A* **2000**, *289*, 217–227. [[CrossRef](#)]
- Tzimas, E.; Zavaliangos, A. Evolution of near-equiaxed microstructure in the semisolid state. *Mater. Sci. Eng. A* **2000**, *289*, 228–240. [[CrossRef](#)]
- Song, Y.B.; Park, K.T.; Hong, C.P. Grain refinement of 6061 Al alloy by the modified strain-induced melt-activated (SIMA) process for semi-solid processing. *Mater. Trans.* **2006**, *47*, 1250–1256. [[CrossRef](#)]
- Parshifard, E.; Shabestari, S.G. An investigation on the microstructural evolution and mechanical properties of A380 aluminum alloy during SIMA process. *J. Alloys Compd.* **2011**, *509*, 9654–9658. [[CrossRef](#)]
- Paes, M.; Zoqui, E.J. Semi-solid behavior of new Al–Si–Mg alloy for thixoforming. *Mater. Sci. Eng. A* **2005**, *406*, 63–73. [[CrossRef](#)]
- Lin, C.W.; Hung, F.Y.; Lui, T.S.; Chen, L.H. High-temperature deformation resistance and forming behavior of two-step SIMA-processed 6066 alloy. *Mater. Sci. Eng. A* **2016**, *659*, 143–157. [[CrossRef](#)]
- Lin, C.W.; Hung, F.Y.; Lui, T.S.; Chen, L.H. Microstructure evolution and high-temperature compressibility of modified two-step strain-induced melt activation-processed Al–Mg–Si aluminum alloy. *Metals* **2015**, *6*, 113. [[CrossRef](#)]
- Lin, C.W.; Hung, F.Y.; Lui, T.S.; Chen, L.H. High-temperature compressive resistance and mechanical properties improvement of strain-induced melt activation-processed Al–Mg–Si aluminum alloy. *Metals* **2016**, *6*, 183. [[CrossRef](#)]
- Hatch, J.E. *Aluminum: Properties and Physical Metallurgy*; American Society for Metals: Materials Park, OH, USA, 1984; pp. 224–240.
- Totten, G.E.; Mackenzie, D.S. *Handbook of Aluminum-Physical Metallurgy and Process*; Metal Dekker Inc.: Valley Forge, PA, USA, 2003; pp. 168–185.
- Zhen, L.; Fei, W.D.; Kang, S.B.; Kim, H.W. Precipitation behavior of Al–Si–Mg alloys with high silicon content. *J. Mater. Sci.* **1997**, *32*, 1895–1902. [[CrossRef](#)]
- Jeniski, R.A., Jr. Effects of Cr addition on the microstructure and mechanical behavior of 6061-T6 continuously cast and rolled redraw rod. *Mater. Sci. Eng. A* **1997**, *237*, 52–64. [[CrossRef](#)]
- Claves, S.R.; Elias, D.L.; Misiolek, W.Z. Analysis of the intermetallic phase transformation occurring during homogenization of 6xxx aluminum alloys. *Mater. Sci. Forum* **2002**, *396*, 667–674. [[CrossRef](#)]
- Miao, W.F.; Laughlin, D.E. Effects of Cu content and presaging on precipitation characteristics in Aluminum alloy 6022. *Metall. Mater. Trans. A* **2000**, *31*, 361–371. [[CrossRef](#)]
- Man, J.; Jing, L.; Jie, S.G. The effects of Cu addition on the microstructure and thermal stability of Al–Si–Mg alloy. *J. Alloys Compd.* **2007**, *437*, 146–150. [[CrossRef](#)]
- Sepehrband, P.; Mahmudi, R.; Khomamizadeh, F. Effect of Zr addition on the aging behavior of A319 aluminum cast alloy. *Scr. Mater.* **2005**, *52*, 253–257. [[CrossRef](#)]

18. Cabibbo, M.; Evangelista, E.; Scalabroni, C.; Bonetti, E. A transmission electron microscopy study of the role of Sc + Zr addition to a 6082-T8 alloy subjected to equal channel angular pressing. *Mater. Sci. Forum* **2006**, *503–504*, 841–846. [[CrossRef](#)]
19. Wang, Z.; Ji, Z.; Hu, M.; Xu, H. Evolution of the semi-solid microstructure of ADC12 alloy in a modified SIMA process. *Mater. Charact.* **2011**, *62*, 925–930. [[CrossRef](#)]
20. Yan, G.; Zhao, S.; Ma, S.; Shou, H. Microstructural evolution of A356.2 alloy prepared by the SIMA process. *Mater. Charact.* **2012**, *69*, 45–51. [[CrossRef](#)]
21. Hardy, S.C.; Voorhees, P.W. Ostwald ripening in a system with a high volume fraction of coarsening phase. *Metall. Trans. A* **1988**, *19*, 2713–2721. [[CrossRef](#)]
22. Huang, H.J.; Cai, Y.H.; Cui, H.; Huang, J.F.; He, J.P.; Zhang, J.S. Influence of Mn addition on microstructure and phase formation of spray-deposited Al-25Si-xFe-yMn alloy. *Mater. Sci. Eng. A* **2009**, *502*, 118–125. [[CrossRef](#)]



© 2017 by the authors. Licensee MDPI, Basel, Switzerland. This article is an open access article distributed under the terms and conditions of the Creative Commons Attribution (CC BY) license (<http://creativecommons.org/licenses/by/4.0/>).